



Article

Cite this article: Chen Z, Cao P, Wang H, Yang H, Yin Q (2024). Theoretical and experimental study on cutting temperature in the presence of drilling fluid during ice-core drilling. *Journal of Glaciology* **70**, e43, 1–12. <https://doi.org/10.1017/jog.2024.2>

Received: 10 June 2023

Revised: 13 December 2023

Accepted: 5 January 2024

Keywords:

cutting experiments; cutting temperature; drilling fluid; ice-core drilling; warm ice

Corresponding author:

Qilei Yin;

Email: yinqilei@jlu.edu.cn

Theoretical and experimental study on cutting temperature in the presence of drilling fluid during ice-core drilling

Zhuo Chen¹ , Pinlu Cao^{1,2} , Han Wang¹, He Yang¹ and Qilei Yin²

¹Polar Research Center, Jilin University, No. 938 Ximinzhu Str., Changchun City 130061, China and

²College of Construction Engineering, Jilin University, No. 938 Ximinzhu Str., Changchun City 130061, China

Abstract

Warm ice at temperatures close to the pressure melting point is often encountered in deep ice-core drilling. The heat generated by rotary cutting can melt ice chips, which seriously threatens the safety of drilling if the chips refreeze on the drill bit or barrel. Lowering the cutting heat is an effective method to reduce the melting of ice chips. In this study, a general theoretical model was established based on heat transfer theory and the cutting mechanism to calculate and analyze the cutter temperature during the circulation of the drilling fluid. The model was validated by a series of experiments, which demonstrated reasonable agreement between the calculated data and experimental results, with a maximum error of <16%. The factors that contribute to the rise in the cutter temperature during warm ice drilling were investigated. Results suggest that the drilling fluid has excellent cooling performance, and its type and flow rate have minimal impact on the cutter temperature. To mitigate the cutter temperature rise, maximizing the rake angle and thermal conductivity of the cutter, while minimizing the rotation speed of the drill bit, cutting depth, cutter width and friction coefficient between the ice and cutter is recommended.

1 Introduction

Deep polar ice preserves valuable records of paleoclimate information, along with information pertaining to the impact of human activities on the natural environment and information on biogeochemical cycles, volcanic activities, cosmic events, biological activities and vegetation evolution over different periods (Beer and others, 1988; Yao and others, 2008; Steinhilber and others, 2012; Cao and others, 2018; Zhong and others, 2021). However, drilling deep into ice using an electromechanical drill often presents significant challenges, commonly known as the warm ice problem (Talalay and others, 2015; Cao and others, 2020). In warm ice, where the temperature is close to or at the pressure melting point, the heat generated during the drilling process can easily melt or partially melt ice chips. If these chips refreeze on the cutters and shoes of the drill bit, it can severely deteriorate the drill performance, leading to a reduced penetration rate, obstructed drilling fluid circulation and potentially hazardous situations, such as a stuck drill (Pattyn, 2010; Kotlyakov and others, 2013). The above-mentioned difficulties during drilling in warm ice have been encountered in numerous ice drilling projects such as NorthGRIP in Greenland (refrozen ice stuck to the drill bit at 2984 m), Dome Fuji in Antarctica (the temperature of ice reached -2.0°C , and the ice refroze at over 3034 m) and Aurora Peak (the cutters were packed with water-bearing ice chips), as illustrated in Figure 1 (Truffer and others, 1999; Takeuchi and others, 2004; Matoba and others, 2014; Talalay, 2016; Motoyama and others, 2021).

Cutting heat is a direct factor that affects the melting of ice chips during warm ice drilling. An effective approach for cooling the cutters is drilling fluid circulation, which can also carry ice chips out of the borehole bottom and balance the pressure. This method is often employed in other areas such as metal and rock cutting (Shokrani and others, 2012; Debnath and others, 2014). Several studies pertaining to metal cutting (Mia and Dhar, 2018; Fang and others, 2020; Lu and others, 2020; Javidikia and others, 2021) have revealed that the coolant plays a vital role in reducing the cutting temperature, decreasing cutter wear and improving its durability. Kishawy and others (2005) studied the effects of dry cutting and flood coolant on the surface roughness and cutting force, and verified the lubricating and cooling effects of the coolant during the cutting process. However, the cutting temperature and heat exchange were not considered in their work. Zhang and others (2020) analyzed the distribution of temperature and stress fields on polycrystalline diamond compact (PDC) bits during rock breaking using the finite-element method, while they ignored drilling fluid circulation. Gorman and others (2014) proposed a method for determining the temperature within a borehole and surrounding rock and discovered that the coolant temperature varied at different locations within the borehole. Che and others (2012) analyzed the temperature rise, stress distribution and force issues related to cutting rocks with PDC bits based on a theoretical investigation and verified them experimentally using thermocouple temperature measurements under dry cutting conditions. Appl and others (1993) measured cutter forces and temperatures separately under air jet, air mist and water jet conditions through tests and demonstrated that the fluid flow exhibited cooling and friction-reducing properties. However, the mechanism of the cooling process has not yet been analyzed or discussed in sufficient detail.

© The Author(s), 2024. Published by Cambridge University Press on behalf of International Glaciological Society. This is an Open Access article, distributed under the terms of the Creative Commons Attribution licence (<http://creativecommons.org/licenses/by/4.0/>), which permits unrestricted re-use, distribution and reproduction, provided the original article is properly cited.

cambridge.org/jog



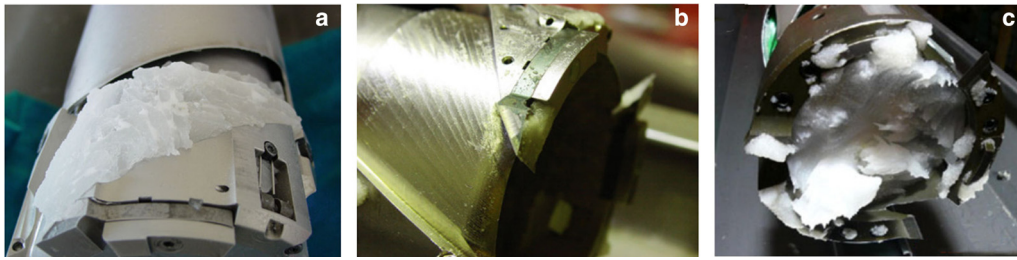


Figure 1. Drilling problems in warm ice drilling. (a) Drill bit accumulated with ice during warm ice drilling, Dome C, Antarctica. (b) Refrozen chips adhered to the cutter, NorthGRIP-2 borehole. (c) Refrozen chips of subglacial water on cutter mounts at depths of 3035.22 m, Dome Fuji.

In previous studies, research on cutting temperatures has been primarily focused on simulations and experiments. However, theoretical calculations have not been employed that often. Komanduri and Hou (2000, 2001a, 2001b) conducted a theoretical analysis of the shear and frictional heat under dry metal cutting conditions, which provided a foundation for calculating the cutting temperature in the presence of coolant circulation. Li (2006) proposed a fundamental heat transfer equation for convective heat transfer of the coolant during the cutting process without considering specific analysis. A predictive thermal analytical model incorporating multisurface two-phase fluid convection was established to calculate the cutting temperature of Ti-6Al-4V under liquid nitrogen cooling (Wang and others, 2020). Nevertheless, the model could not be utilized in the ice drilling process as heat transfer in ice cutting was only analyzed on the rake side of the cutter, disregarding other surfaces that come into contact with the ice core and borehole. Ortega and others (1984) established a PDC bit temperature prediction model for drilling-fluid circulation based on experimental data. Convective heat transfer coefficients used in the model were obtained solely based on the test results, and therefore, the application of the model was restricted under other cutting conditions. Hence, the above-mentioned studies cannot be applied to ice drilling directly.

Furthermore, recent studies have primarily focused on the cutting temperature in ice-core drilling under dry conditions rather than under drilling fluid circulation. Azuma and others (2007) proposed a theoretical model of cutting temperatures without drilling fluid and revealed the primary sources and factors affecting the cutting temperature. Cao and others (2015) conducted experimental tests on temperature variation during cutting and analyzed the effects of various factors such as the drill bit pressure, rotation speed and rake angle of the cutter on the cutting temperature. Although an in-depth analysis was not performed, they surmised that the drilling fluid demonstrated a cooling effect. To investigate the impact of the drilling fluid on cutting heat and cutter temperature, a theoretical model was developed based on

heat transfer theory and previous research on metal and rock cutting. The model focuses on heat dissipation in a single cutter due to drilling fluid. To validate the theoretical model, a series of experiments were conducted. The analysis process includes consideration of several factors such as material properties and drilling parameters.

2 Theoretical analysis

A single cutter of the drill bit was selected as the research object to simplify calculations; to that end, this study made the following assumptions:

- (1) Ice is assumed to possess isotropic and uniform physical properties.
- (2) The influence of heat on the physical properties of ice and the cutter is ignored.
- (3) All energy consumed during the drilling process is converted into heat.
- (4) The heat generated by friction between the flank surface of the cutter and ice is negligible.

2.1 Cutting heat

The analytical model used to estimate the heat transfer between the single cutter and ice during the drilling process is illustrated in Figure 2. The cutting model of the drill bit shown in Figure 2a was simplified to obtain the cutting model of a single cutter, as shown in Figure 2b. The cutting heat primarily results from shear deformation and frictional heat between the ice chip and cutter (Komanduri and Hou, 2001c):

$$Q_c = Q_s + Q_f, \quad (1)$$

where Q_c , Q_s and Q_f denote the heat generated by the cutting process, shearing and friction, respectively.

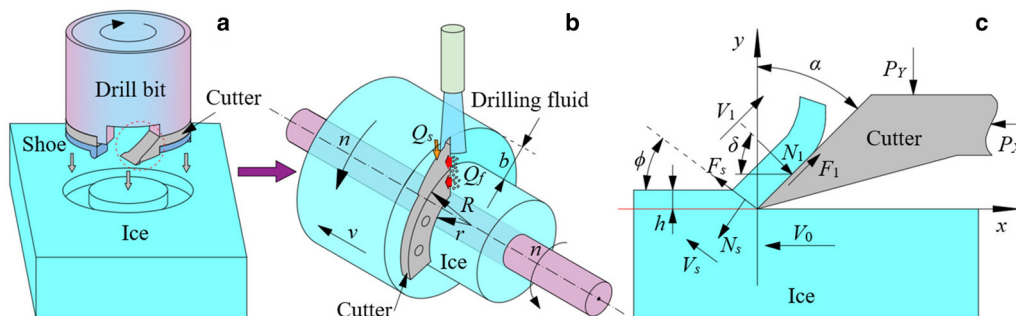


Figure 2. Mechanical and heat transfer models of a single cutter: (a) cutting model of the drill bit, (b) simplified cutting model of a single cutter and (c) mechanical analysis of a single cutter. See main text for an explanation of the quantities shown.

Based on the mechanical analysis shown in Figure 2c (Shan and others, 2019; Veiga and others, 2021), the calculation formula for each heat component can be expressed as follows:

$$Q_s = F_s V_s = \frac{\pi n(r + R) \cos \alpha \cos(\phi + \delta - \alpha)(P_X \cos \delta - P_Y \sin \delta)}{60 \cos(\phi - \alpha) \cos(\alpha - 2\delta)}, \quad (2)$$

$$Q_f = F_1 V_1 = \frac{\pi n(r + R) \sin \phi [P_X \sin 2\delta - 2P_Y (\sin \delta)^2]}{120 \cos(\phi - \alpha) \cos(\alpha - 2\delta)}, \quad (3)$$

where F_s and F_1 respectively denote the shear force and friction in N; V_s and V_1 respectively denote the shear velocity and moving speed of ice chips in m s^{-1} ; P_Y and P_X respectively denote the axial and horizontal cutting forces in N; n denotes the rotation speed in r min^{-1} ; R and r respectively denote the outer and inner diameters of the cutter in m; ϕ denotes the angle between the horizontal and shear plane (i.e. shear angle) in rad; α denotes the rake angle in rad; δ denotes the surface friction angle in rad.

2.2 Relationship between cutting heat and temperature

According to the correlation formula for ice cutting under dry conditions (Azuma and others, 2007), the temperature rise of the cutter can be expressed as

$$\Delta T_s = \frac{0.754}{k_1 \sqrt{V_0 \epsilon h / 4 \lambda_i}} R_1 \frac{Q_s}{2b}, \quad (4)$$

$$\Delta T_f = \frac{0.377 R_2 Q_f}{k_i b \sqrt{V_1 l_f / 4 \lambda_i}}, \quad (5)$$

where ΔT_s and ΔT_f respectively denote the temperature rise caused by shearing and friction in $^\circ\text{C}$, k_1 and k_i respectively denote the thermal conductivities of the cutter and ice in $\text{W (m }^\circ\text{C)}^{-1}$, b denotes the width of the cutter in m, l_f denotes the contact length between the ice chips and cutter in m, λ_i denotes the thermal diffusion coefficient of ice in m s^{-1} , R_1 and R_2 represent proportional coefficients of heat transfer to the cutter, h denotes the cutting depth in m; ϵ denotes chip deformation, which is dimensionless and the other parameters are as previously described.

Therefore, the temperature of the cutter T_c can be given by

$$T_c = T_i = \Delta T + T_0 = \Delta T_s + \Delta T_f + T_0, \quad (6)$$

where T_i and T_0 denote the temperature of ice chips and ambient temperature in $^\circ\text{C}$, respectively.

2.3 Heat exchange and temperature of the cutter under drilling fluid circulation

Heat exchange occurs when drilling fluid flows on the surface of a cutter. This can be simplified as convective heat transfer on a 1-D swept flat plate. Assuming that the drilling fluid is an incompressible Newtonian fluid with no internal heat source and constant physical properties, heat dissipation caused by viscous friction appears negligible. According to Fourier's law of heat conduction and the differential equations of convective heat transfer, the heat transfer coefficient of the cutter surface, ψ , can be obtained as follows:

$$\psi = 0.664 \frac{k_{df}}{l_c} \left(\frac{V_{df} l_c}{\nu_{df}} \right)^{1/2} \left(\frac{\mu_{df} c_{df}}{k_{df}} \right)^{1/3}, \quad (7)$$

where k_{df} denotes the thermal conductivity of the drilling fluid in $\text{W (m }^\circ\text{C)}^{-1}$, V_{df} denotes the flow rate of the drilling fluid in m s^{-1} , l_c denotes the length of the cutter in m, ν_{df} denotes the kinematic viscosity of the drilling fluid in $\text{m}^2 \text{s}^{-1}$, μ_{df} denotes the dynamic viscosity of the drilling fluid in Pa s and c_{df} denotes the specific heat capacity of the drilling fluid in $\text{J (kg }^\circ\text{C)}^{-1}$.

Based on Newton's law of cooling, the amount of heat removed by the drilling fluid from the cutter per unit of time is described as follows:

$$q_t = \psi(T_c - T_{df})A. \quad (8)$$

The heat exchange area A between the drilling fluid and cutter is simplified as

$$A = l_c b. \quad (9)$$

The heat exchange time t between the drilling fluid and cutter is described as

$$t = \frac{l_c}{V_{df}}. \quad (10)$$

The heat Q_t absorbed by the drilling fluid in t time is calculated as follows:

$$Q_t = q_t t = 0.664 \frac{k_{df}}{l_c} \left(\frac{V_{df} l_c}{\nu_{df}} \right)^{1/2} \left(\frac{\mu_{df} c_{df}}{k_{df}} \right)^{1/3} (T_c - T_{df}) l_c b \frac{l_c}{V_{df}}. \quad (11)$$

According to the heat transfer theory, the heat Q_t eliminated by the drilling fluid at t time is given as follows:

$$Q_t = c_{df} m_{df} \Delta T_{df}. \quad (12)$$

The mass of the drilling fluid on the cutter surface is as follows:

$$m_{df} = \rho_{df} l_c b d_s, \quad (13)$$

where T_{df} denotes the drilling fluid temperature in $^\circ\text{C}$, ρ_{df} denotes the density of the drilling fluid in kg m^{-3} , d_s denotes the average thickness of the drilling fluid on the cutter surface in m and the other parameters are as previously described.

The average temperature rise of the drilling fluid on the cutter surface can be deduced from Eqns (11)–(13):

$$\Delta T_{df} = \frac{0.664 (k_{df}/l_c) ((V_{df} l_c)/\nu_{df})^{1/2} ((\mu_{df} c_{df})/k_{df})^{1/3} (T_c - T_{df}) (l_c/V_{df})}{c_{df} \rho_{df} d_s}. \quad (14)$$

The average temperature of the drilling fluid on the cutter surface after heat absorption is expressed as

$$T_{df} = T_{df0} + \Delta T_{df} = T_{df0} + \frac{0.664 (k_{df}/l_c) ((V_{df} l_c)/\nu_{df})^{1/2} ((\mu_{df} c_{df})/k_{df})^{1/3} (T_c - T_{df}) (l_c/V_{df})}{c_{df} \rho_{df} d_s}, \quad (15)$$

where T_{df0} denotes the initial temperature of the drilling fluid on the cutter surface in $^\circ\text{C}$.

The heat transfer process can be regarded as flat-wall steady-state heat conduction with steady heat transfer owing to the relative stability of the two heat sources under stable conditions. In addition, the temperature change during the cutting process primarily occurs along the thickness direction of the cutter instead of the length and width. Thus, it can be regarded as a 1-D heat conduction problem formulated with reasonably simplified boundary conditions based on a realistic cutting process. So the following equation can be given as

$$\frac{\partial^2 t}{\partial x^2} = 0. \tag{16}$$

Substituting conditions wherein temperature T ranges from T_{df} to T_c when x ranges from 0 to d into Eqn (16) yields

$$T_x = T_{df} - (T_{df} - T_c) \frac{x}{d}, \tag{17}$$

where T_x denotes the temperature at an arbitrary point in the cutter in °C, x denotes the coordinate value of an arbitrary point in the cutter in m and d denotes the thickness of the cutter in m.

The average temperature of the cutter in the presence of the drilling fluid can be obtained by calculating the definite integral of Eqn (17):

$$T_{ac} = \frac{\int_0^d T_x dx}{d} = \frac{\int_0^d [T_{df} - (T_{df} - T_c)(x/d)] dx}{d} = \frac{T_{df} + T_c}{2}. \tag{18}$$

Substituting Eqn (6) and Eqn (15) into Eqn (18) yields

$$T_{ac} = \frac{1}{2} \left[T_{df0} + \frac{0.664(k_{df}/l_c)((V_{df}l_c)/v_{df})^{1/2}((\mu_{df}c_{df})/k_{df})^{1/3}(T_c - T_{df})}{c_{df}\rho_{df}d_s} + T_0 + \frac{0.754}{k_1\sqrt{L_1}}R_1\frac{Q_s}{2b} + \frac{0.377R_2Q_{f1}}{k_1b\sqrt{V_1l_f/4\lambda_i}} \right]. \tag{19}$$

The average temperature rise ΔT_c of the cutter in the presence of drilling fluid during drilling is expressed as

$$\Delta T_c = T_{ac} - T_0. \tag{20}$$

The relevant parameters in Eqn (19) can be expressed as follows:

$$R_1 = \frac{1.33\sqrt{\lambda_i\varepsilon/V_0h}}{1 + 1.33\sqrt{\lambda_i\varepsilon/V_0h}}, \tag{21}$$

$$R_2 = \frac{0.377Q_f/(bk_i\sqrt{V_1l_f/4\lambda_i}) + \Delta T_s}{(Q_f/bk_c)\Lambda + 0.377Q_f/(bk_i\sqrt{V_1l_f/4\lambda_i})}, \tag{22}$$

$$\varepsilon = \frac{\cos \alpha}{\sin \phi \cos(\phi - \alpha)}, \tag{23}$$

$$\phi = \frac{\pi}{4} + \alpha - \delta, \tag{24}$$

$$\Lambda = \frac{2}{\pi} \left\{ \sin h^{-1} \left(\frac{b}{2l_f} \right) + \frac{b}{2l_f} \sin h^{-1} \left(\frac{2l_f}{b} \right) + \frac{1}{3} \left(\frac{b}{2l_f} \right)^2 + \frac{1}{3} \left(\frac{2l_f}{b} \right) - \frac{1}{3} \left(\frac{b}{2l_f} + \frac{2l_f}{b} \right) \left[1 + \left(\frac{b}{2l_f} \right)^2 \right]^{1/2} \right\}, \tag{25}$$

$$l_f = \frac{h \sin(\phi + \delta - \alpha)}{\sin \phi \cos \delta}, \tag{26}$$

where Λ represents the shape factor of a moving plane heat source, and it is dimensionless; and the other parameters are as described above.

Through the mathematical description of the theoretical model, the intrinsic heat transfer mechanism between the drilling fluid and cutter during the process of ice cutting can be elucidated. According to the model, various factors such as the drilling parameters, drilling fluid parameters, environmental factors and geometric dimensions of the cutter can influence the cutting heat. The flow rate of the drilling fluid and its thermophysical parameters are closely related to the cooling process.

3 Experimental equipment

3.1 Experimental device

Figure 3 depicts a schematic of the experimental device used to monitor the temperature during rotary cutting. A single cutter fixed to the guideway can be moved horizontally and is controlled by an electric draw stem with a maximum stroke of 550 mm. The displacement and speed of the draw stem are continuously monitored using an MT pull-wire displacement sensor, which has a range of 0–1000 mm and an accuracy of 1 mm. The motor drives the rotation of the ice core connected to the motor via a flange. The rotation speed is monitored by the GM8905 rotation speed sensor with an accuracy of 0.1 r min⁻¹. The drilling fluid, circulated by a pump placed in a reservoir under the ice core, continuously cools the cutter at a flow rate of 20 L min⁻¹. The fluid

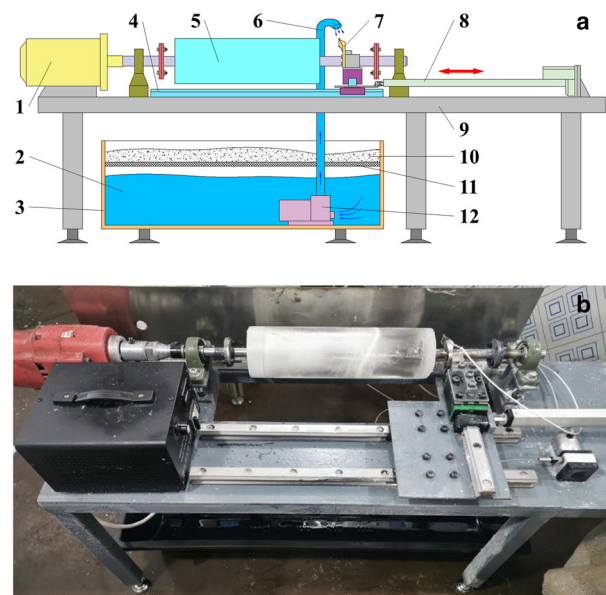


Figure 3. (a) Schematic and (b) image of the measurement apparatus: (1) motor; (2) drilling fluid; (3) reservoir; (4) guideway; (5) ice; (6) pipe; (7) cutter; (8) electric draw stem; (9) base frame; (10) ice chip; (11) screen; (12) pump.

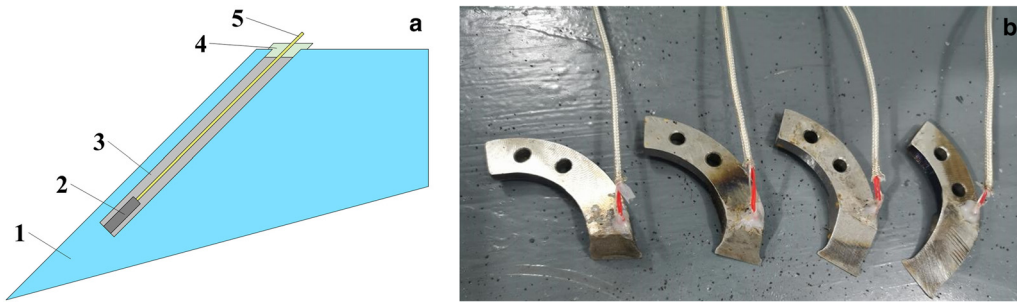


Figure 4. (a) Layout and (b) image of the cutter thermoresistor: (1) cutter; (2) sensor probe; (3) silicone grease; (4) insulation glue; (5) sensor wire.

carrying the ice chip falls back to the reservoir under gravity. The reservoir is equipped with a screen to filter the ice chips.

To measure the cutting temperature, a PT100 thermoresistor is used, which has an accuracy of 0.1°C and a temperature range of -50 to 200°C . It is placed in a hole filled with silicone grease and close to the rake face of the cutter, which records temperature during the experimental procedure (Fig. 4). Similar applications of this silicone grease have been carried out in temperature measurement processes in other fields (Xu and others, 2020), demonstrating that the impact on temperature monitoring can be disregarded. The diameter and depth of the hole are 3 mm and half of the cutter length respectively, and the wall thickness from the rake face is 0.5 mm. The inner and outer diameters of the cutter are 60 and 100 mm, respectively.

The above parameters were monitored during the cutting process in real time.

3.2 Ice sample preparation

The ice sample investigated in this study was prepared from purified water in circular steel tubes. The steel tubes contained a central cylinder with steel sheets, which could maintain a coaxial connection between the ice core and the motor. The steel sheets could increase the bonding strength between the ice core and cylinder. The preparation procedure for the ice core is presented in Figure 5. To prepare the ice samples, purified water was poured into steel tubes sealed by rubbers, which were then placed in a cold room with an adjustable temperature range of 0 to -30°C and an increment of 0.1°C . Once the water was completely frozen, the steel tubes were removed from the cold room and placed in an outdoor environment with a temperature of 20°C for several minutes to allow the ice surface to melt. Subsequently, the ice samples were taken from the steel tubes, and the samples were then placed in the cold room again to cool them to the desired test temperature. This procedure allowed for easy removal of the ice samples from the steel tubes while maintaining their structural integrity.

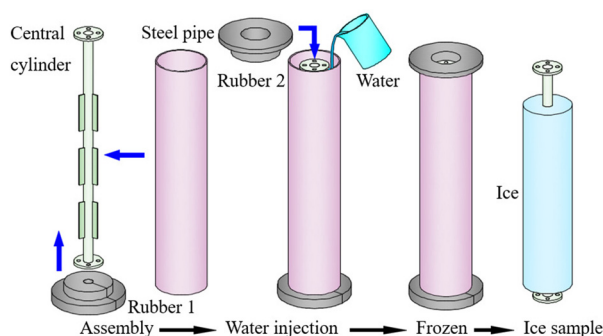


Figure 5. Preparation procedure of ice samples with 100 mm in diameter and 400 mm in length.

The diameters and lengths of the samples were 100 and 400 mm, respectively.

3.3 Testing procedure

The experiment was conducted in the cold room. After installing the ice core, we adjusted the rotation rate of the motor and the feeding speed of the electric draw stem to maintain it at a fixed value. Following this, we carried out a series of experiments on cutting ice cores with different cutters using the aforementioned device (Section 3.2) to validate the reliability of the theoretical model. It was necessary to maintain an interval of 30 min between each group of tests to lower the temperature of the cutter, which increased owing to an increase in the temperature during the cutting process. During the experiments, the drilling fluid was circulated on the surface of the cutter, and data acquisition software was used for real-time monitoring.

Aviation kerosene was utilized as the drilling fluid at a flow rate of 20 L min^{-1} . The thermophysical parameters of the drilling fluid, ice and cutters are listed in Table 1. A dash sign means that the property is not applicable to the material. A total of 55 test groups were executed, incorporating the factors detailed in Table 2, and each group of tests was repeated at least three times to obtain accurate results. The cutter parameters that we used in the theoretical and experimental analysis are shown in Table 3.

4 Results and discussion

4.1 Freezing and cooling time for ice samples

To ensure complete freezing of purified water and temperature equilibration with the environment during testing, it is necessary to determine the freezing time and cooling rate by means of an ice sample thermometry test, as shown in Figure 6. Figure 7a shows the temperature variation during freezing at -10°C , measured with a thermocouple placed near the central cylinder of the water sample.

Owing to the interface instability and the influence of surface energy, the water in contact with the central cylinder and steel pipe froze earlier than that in the middle position. This process with an approximately constant temperature corresponded to the initial stage of the curve, which took $\sim 15\text{ h}$. A phase transition occurred within 15 h, and the temperature decreased sharply to ambient temperature. Previous studies (Cao and others, 2020) have proven that the freezing rate of ice increases with a decrease in the temperature, and the properties of the ice core remain unchanged with an extension in the freezing time after complete freezing. Therefore, the ice core used in subsequent tests was frozen for at least 40 h.

The cooling time of the ice sample from room temperature to the test temperature was measured using the same method, as

Table 1. Thermal properties of the cutter, ice and drilling fluid

Materials	Density kg m ⁻³	Specific heat J (kg °C) ⁻¹	Heat conductivity coefficient W (m °C) ⁻¹	Thermal diffusion coefficient mm ² s ⁻¹	Dynamic viscosity Pa s	Thermal diffusivity
Cutter	1500	230	30	–	–	1.185 × 10 ⁻⁶
Ice	920	2078	2.29	1.2 × 10 ⁻⁶	–	1.24 × 10 ⁻⁶
Drilling fluid	870	1625	0.14	–	0.013	–

Table 2. Experimental parameters

Test temperature: °C	–10	–15	–20	–25
Rake angle: °	15	30	45	60
Rotation speed: r min ⁻¹	80	110	140	200
Penetration rate: mm s ⁻¹	1	1.5	2	2.5

Table 3. Cutter parameters

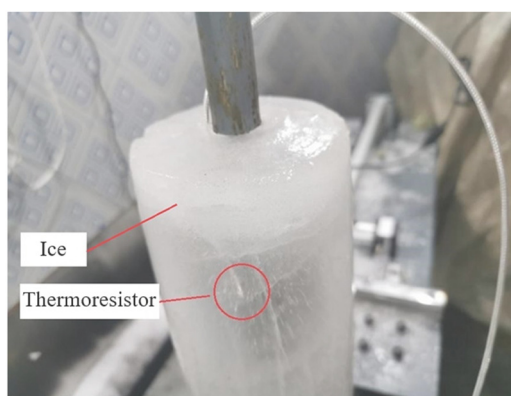
Rake angle°	penetration rate mm s ⁻¹	Rotation speed r min ⁻¹	Thermal conductivity of the cutter W (m °C) ⁻¹	Cutting depth mm	Cutter width mm	Friction coefficient between ice and cutter
45	1.5	110	60	0.8	20	0.06

shown in Figure 7b. Initially, the temperature of the ice sample decreases rapidly due to the large temperature difference, and then the cooling rate slows down as it approaches the ambient temperature. After ~4 h, the temperature of the ice sample reaches equilibrium with the ambient temperature. Therefore, to minimize the influence of the initial temperature, the ice samples were cooled in the testing environment for a minimum of 4 h. All ice samples were held at the test temperature for 5 h prior to testing.

4.2 Validation of the theoretical model

4.2.1 Data processing

The temperature change of the cutters during the drilling process at –10°C is presented in Figure 8. The data derived from the thermoresistor were quite noisy owing to ambient noise and sensor accuracy (0.1°C). The experimental data were fitted using a two-phase exponential association equation embedded in the Origin code. The fitted curve agrees well with the scatter data, as illustrated in Figure 8. It can be seen that the temperature rise of the cutter increases gradually with time, and the heating rate decreases until stabilization, which conforms with the general law of unsteady heat transfer (John and John, 2006). The heat

**Figure 6.** Test to determine the temperature of the ice sample.

source was primarily concentrated on the tool nose and rake face of the cutter, and the heat was transferred to the interior rapidly owing to the initial significant temperature difference. This process, which is affected by the ambient temperature, is referred to as the informal state stage of unsteady heat conduction, as illustrated in region I in Figure 8, and it corresponds to the primary stage of the curve. The subsequent process is referred to as the regular state stage of unsteady heat conduction, wherein the temperature distribution of the cutter is primarily affected by the heat exchange boundary conditions, as illustrated in region II in Figure 8. Finally, the cutting heat reaches equilibrium with the heat carried away by the drilling fluid, and this corresponds to the end stage of the curve.

The temperature rise of the cutter is influenced by several factors, such as the rake angle of the cutter, the rotation speed of the drill bit and the penetration rate, which will be discussed in detail later in this study.

4.2.2 Validation of the theoretical model

To confirm the accuracy of our theoretical model, we selected the point at which the temperature of each set of experiments reached stability in order to investigate the temperature rise of the cutter during the drilling process under various conditions, as illustrated in Figure 9. The results of both the experiments and calculations show that the temperature rise of the cutter increases as the temperature of the ice sample decreases. This is because lower-temperature ice has greater shear strength, which produces more heat during cutting. The calculated and experimental results demonstrate a strong agreement, with a temperature difference of <0.4°C and differences of <16%. A few errors may be caused by the accuracy of the thermoresistor (0.1°C), the minor temperature differences in the ice sample and the way the surface of the cutter is flowed over by the fluid instead of being immersed in it.

Furthermore, Figure 9 illustrates that the temperature increase of the cutter is inversely proportional to its rake angle and directly proportional to the penetration rate and rotation speed of the drill bit.

We investigated the effect of the rake angle α of the cutter on its temperature rise ΔT_c and cutting heat Q_c during drilling using the proposed theoretical model. The results are shown in Figure 10, which demonstrate that both ΔT_c and Q_c decrease as the rake angle α increases, decreasing from 37.6 to 18 J s⁻¹ and from 2.5 to 2.1°C respectively, when α increases from 15° to 60°. The reason for this phenomenon is that increasing α reduces both the shear heat Q_s and the temperature rise ΔT_s of the cutter, as indicated by Eqns (2) and (4). On the other hand, α has little impact on the friction heat Q_f of the cutter, as stated in Eqn (3). However, the temperature rise ΔT_f is positively correlated with α because the proportional coefficient R_2 of frictional heat transfer to the cutter is related to α , as shown in Eqn (22). Since the magnitude of ΔT_s is greater than that of ΔT_f , ΔT_c decreases as α increases. Therefore, increasing the rake angle of the cutter can reduce the cutting temperature. However, a larger rake angle of the cutter corresponds to a thinner thickness, which may affect its strength. It is recommended that the rake angle should be increased as much as possible while maintaining the strength of the cutter. In addition, according to the force analysis of the cutter

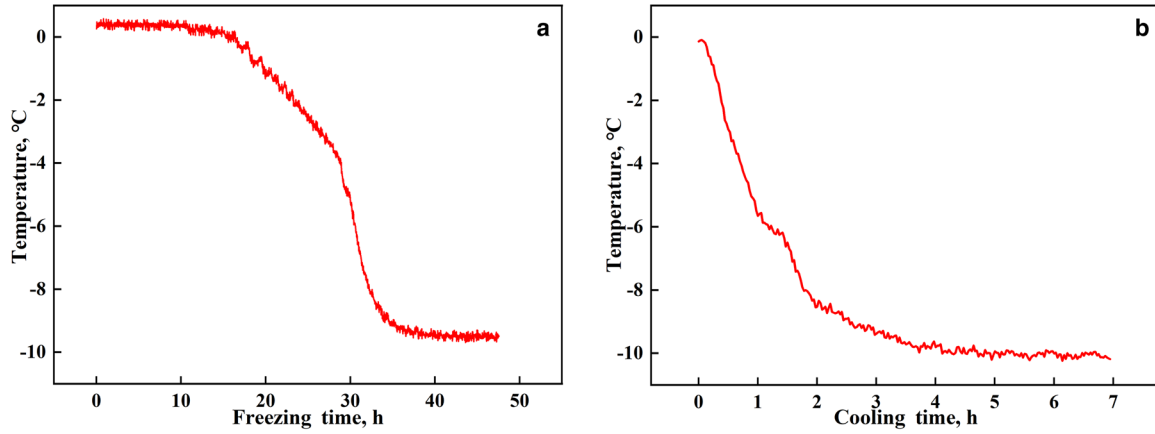


Figure 7. Temperature measurement curve of the ice sample at -10°C : (a) freezing time and (b) cooling time.

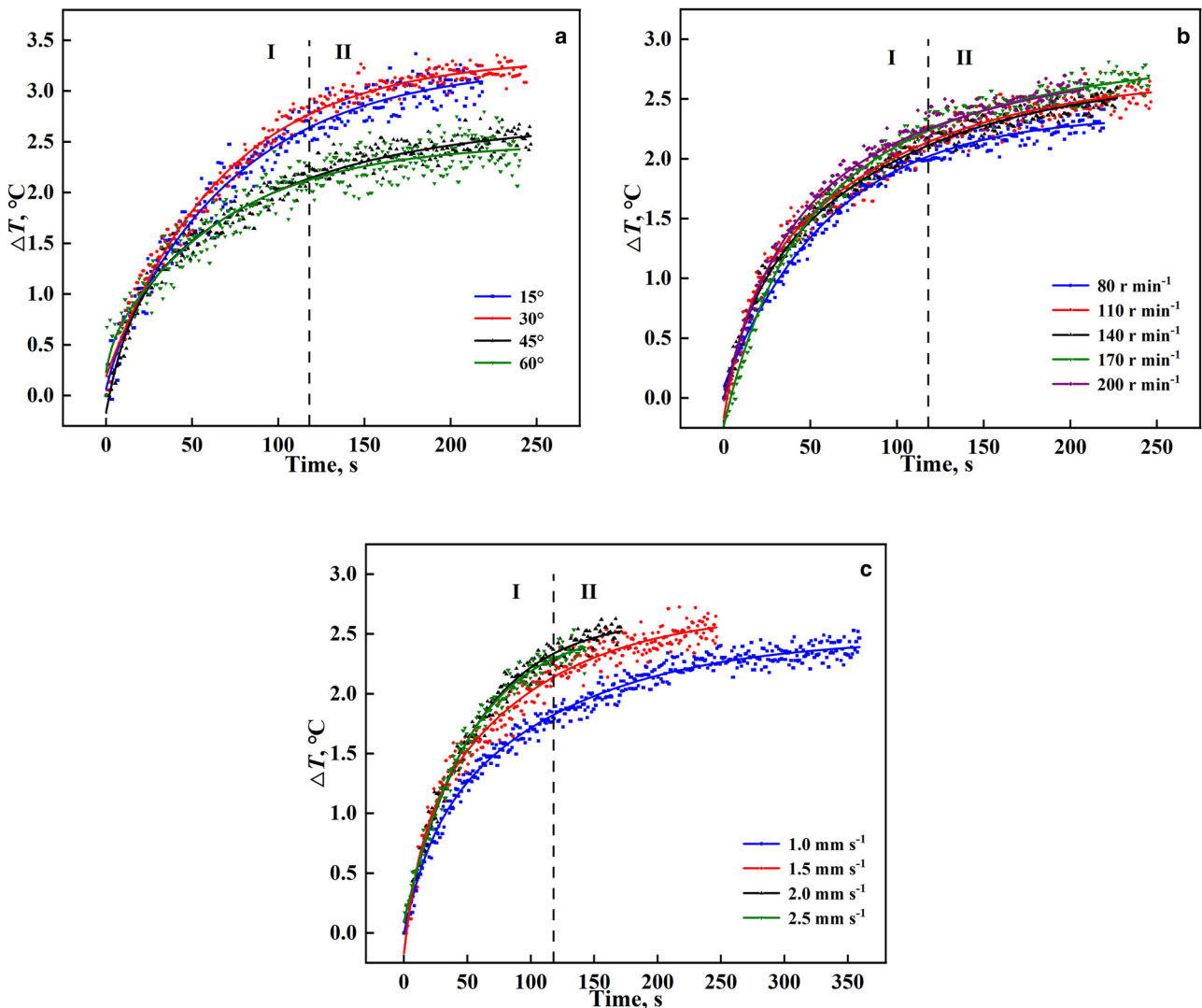


Figure 8. Variation of cutter temperature increase with time during the cutting process: (a) rake angle of the cutter, (b) rotation speed of the drill bit and (c) penetration rate of the drill bit.

(Azuma and others, 2007), the torque decreases with the increase of the rake angle when other parameters are constant, which is favorable for the improvement of the penetration rate.

Figure 11 illustrates a positive correlation between the penetration rate of the drill bit and both the cutting heat Q_c and the temperature rise ΔT_c of the cutter. Increasing the penetration rate

from 1 to 2.5 mm s^{-1} leads to a significant increase in both Q_c and ΔT_c values from 16.0 to 40.0 J s^{-1} and from 2.0 to 2.5°C , respectively. The study found a positive correlation between the penetration rate and cutting depth h during drilling when the rotation speed of the drill bit remains constant. An increase in the value of h results in a higher amount of ice being broken

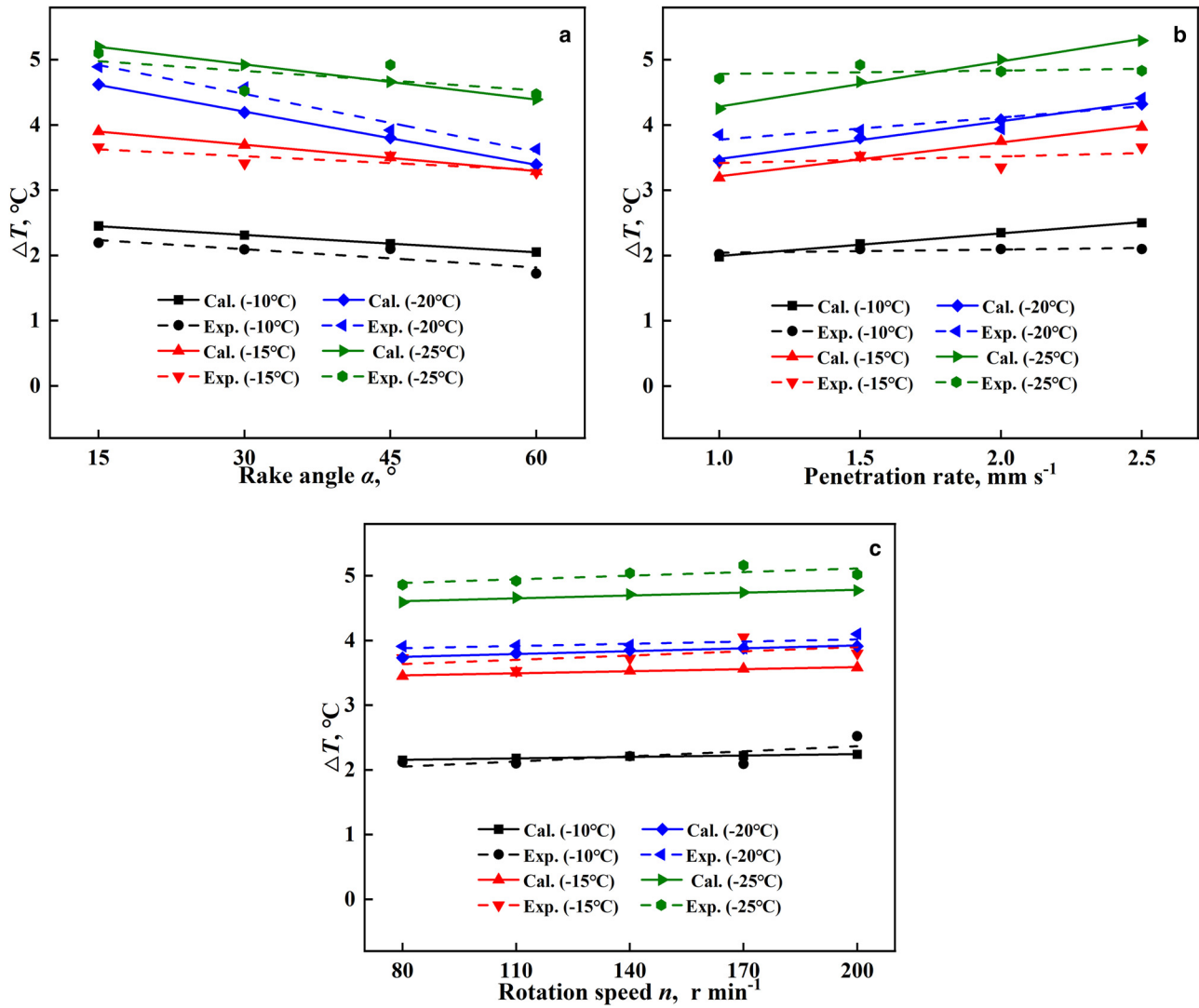


Figure 9. Comparison of test and theoretical calculation results with drilling fluid at -10 , -15 , -20 and -25°C , respectively: (a) rake angle of the cutter, (b) penetration rate of the drill bit and (c) rotation speed of the drill bit.

per unit of time. The increase in the value of h leads to an increase in the horizontal cutting force P_X of the cutter, resulting in an increase in Q_s , Q_b , ΔT_s and ΔT_f values as per Eqns (2)–(5). Thus, it is recommended to decrease the cutting depth of the drill bit when drilling in warm ice.

Figure 12 demonstrates a positive correlation between the value of cutting heat Q_c and the temperature rise ΔT_c of the cutter with the rotation speed n of the drill bit. The values of Q_c and ΔT_c increase from 17.4 to 43.6 J s⁻¹ and from 2.0 to 2.6°C, respectively, as the n value increases from 80 to 200 r min⁻¹. An increase in the value

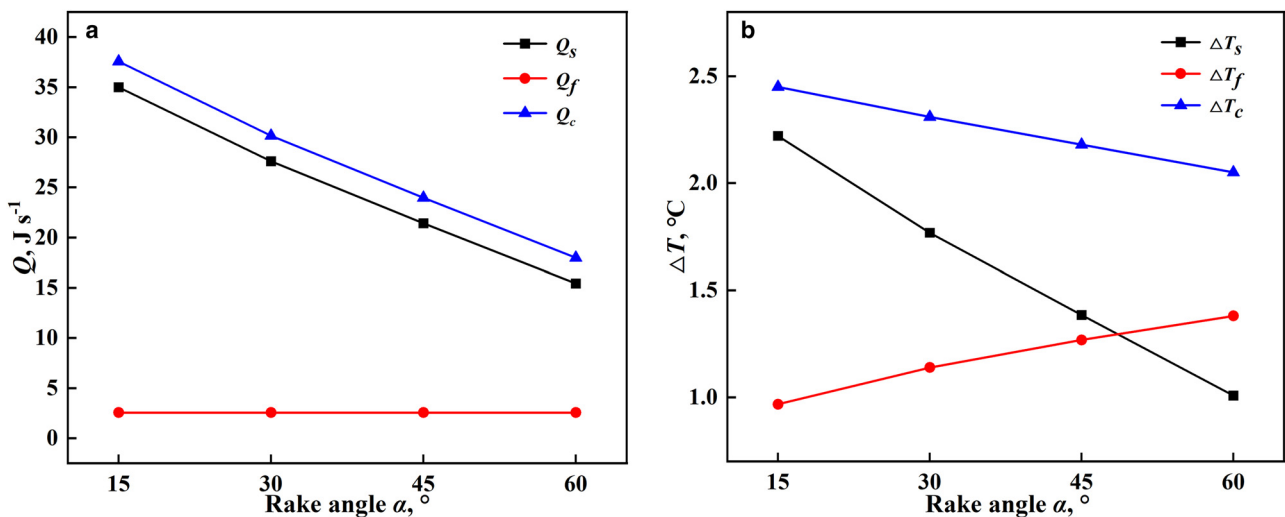


Figure 10. Model cutting heat and temperature rise vs rake angle of the cutter (-10°C): (a) cutting heat and (b) temperature rise of the cutter.

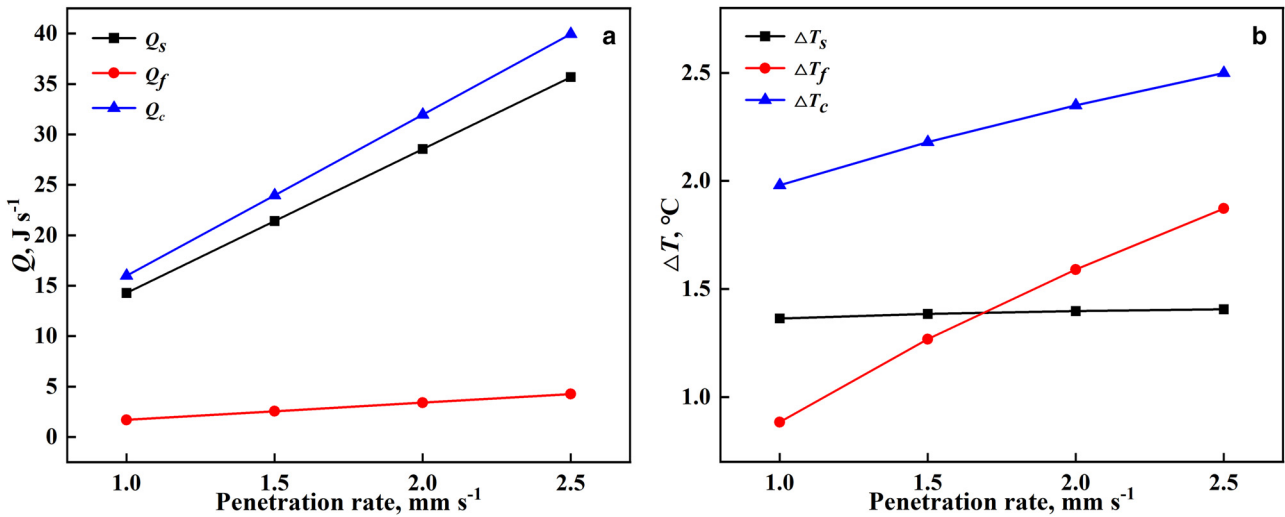


Figure 11. Model cutting heat and temperature rise vs penetration rate: (a) cutting heat and (b) temperature rise of the cutter.

of n leads to a larger amount of ice broken per unit of time, resulting in larger values of Q_s , Q_f , ΔT_s and ΔT_f , as per Eqns (2)–(5). Thus, appropriate reduction of the rotation speed of the drill bit is required to lower the cutting temperature. However, the penetration rate decreases as the rotation speed decreases. It is recommended that the rotation speed should be reduced as much as possible while the penetration rate meets the requirements.

4.3 Influence factors on the temperature rise of the cutter

The parameters that may affect the cutting heat Q_c and temperature rise ΔT_c during the drilling process were discussed in the context of drilling fluid at a temperature of $-10^{\circ}C$, which is similar to the temperature of warm ice.

4.3.1 Drilling fluid

Figure 13a presents the temperature rise of the cutter with and without drilling fluid based on the theoretical model. Kerosene, ethylene glycol and silicon oil are three types of low-temperature drilling fluids generally used in ice drilling. The results indicate that drilling fluids can effectively reduce the temperature rise of the cutter, and the type and flow rate of the fluid have a negligible impact on this reduction. This can be attributed to the efficient

dissipation of cutting heat by the drilling fluid even at lower flow rates while increasing the flow rate beyond $\sim 2 L min^{-1}$ does not yield substantial benefits, as shown in Figure 13b. Nevertheless, it is recommended to use the highest possible flow rate to enhance the carrying capacity of fluid. Otherwise, ice chips may accumulate near the drill bit, leading to reduced penetration rates and an increased risk of a stuck drill.

4.3.2 Cutter width

Figure 14 presents the influence of cutter width on Q_c and ΔT_c , which are critical parameters in the design of drill bits and cutters. As shown, Q_c and ΔT_c increase with an increase in cutter width. Specifically, as the cutter width increases from 10 to 30 mm, Q_c increases from 10.5 to 40.5 $J s^{-1}$ and ΔT_c increases from 2.0 to 2.3 $^{\circ}C$. This is because a larger cutter width results in a greater amount of ice broken per unit of time, leading to higher values of Q_c and ΔT_c . Therefore, in order to reduce cutting heat, the cutter width should be minimized. However, reducing the cutter width will reduce the thickness of the drill bit body, which will affect its strength. And it is not conducive to the installation of other mechanisms such as core catchers (Talalay, 2014). It is recommended to reduce the cutter width based on the actual design requirements.

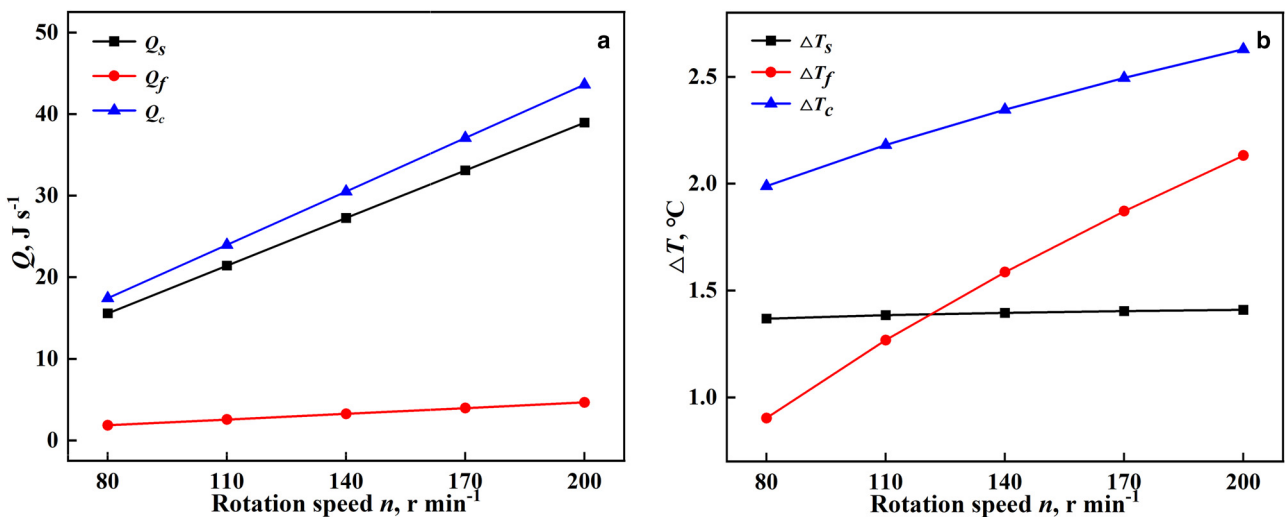


Figure 12. Model cutting heat and temperature rise vs rotation speed of the drill bit: (a) cutting heat and (b) temperature rise of the cutter.

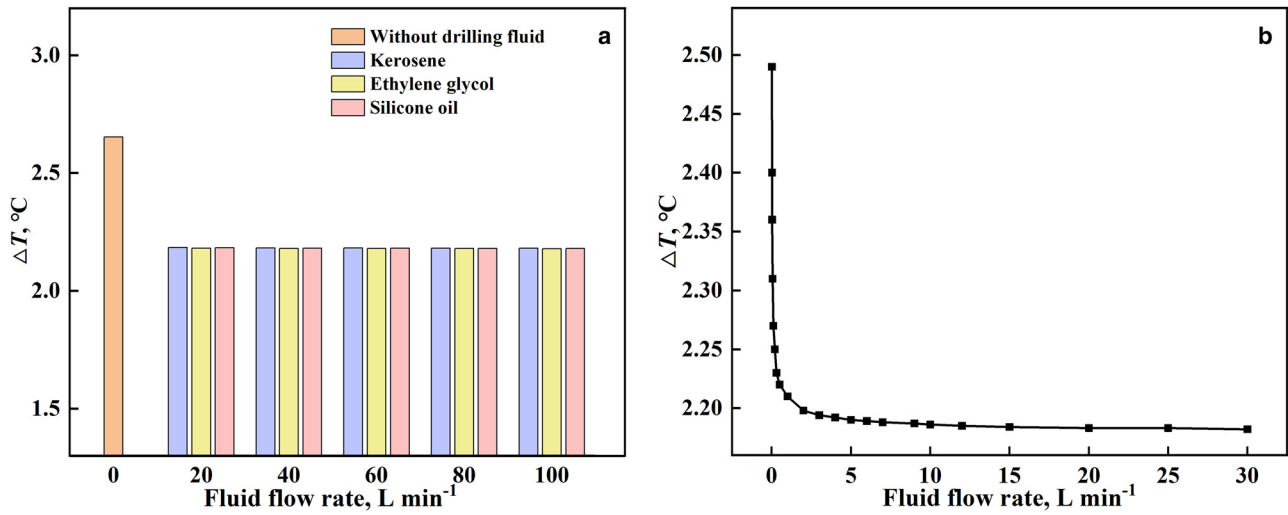


Figure 13. Model temperature rise vs type and flow rate of drilling fluids: (a) type and flow rate of drilling fluids and (b) flow rate of drilling fluid.

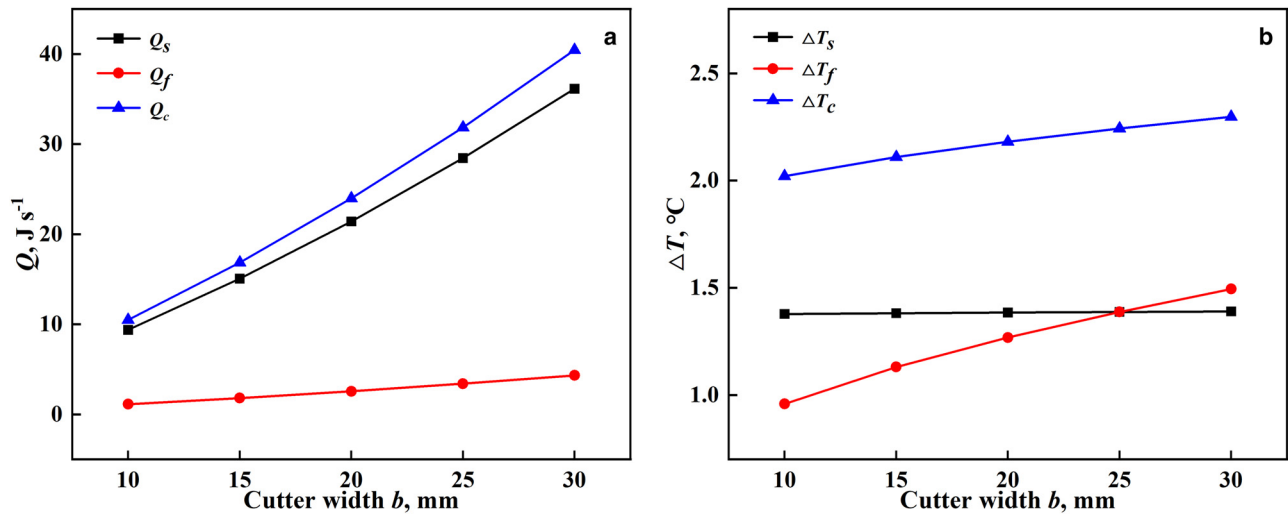


Figure 14. Model cutting heat and temperature rise vs cutter width: (a) cutting heat and (b) temperature rise of the cutter.

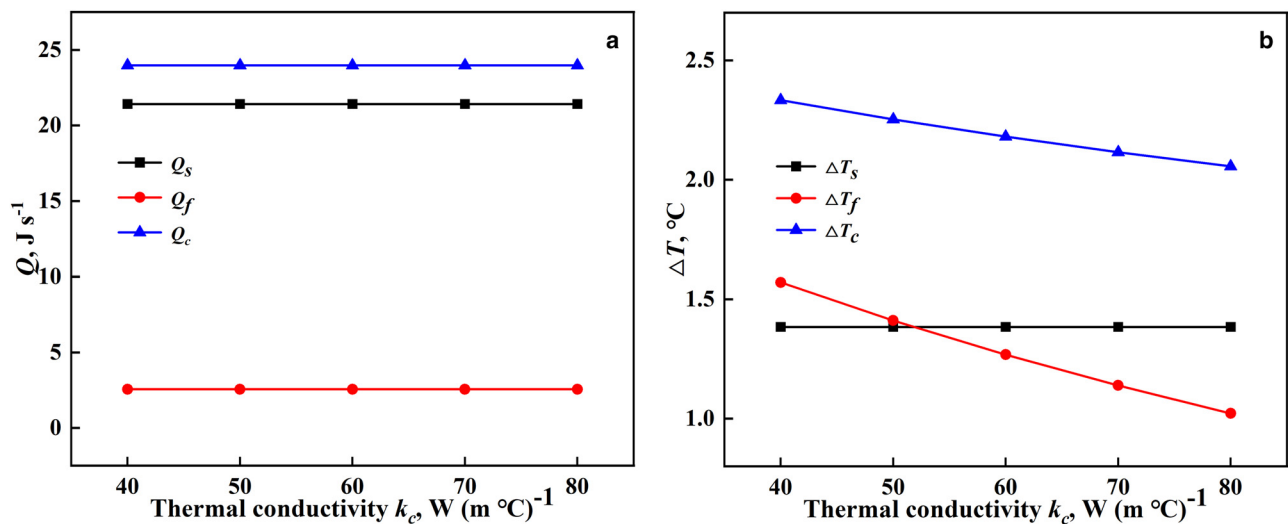


Figure 15. Model cutting heat and temperature rise vs thermal conductivity of the cutter: (a) cutting heat and (b) temperature rise of the cutter.

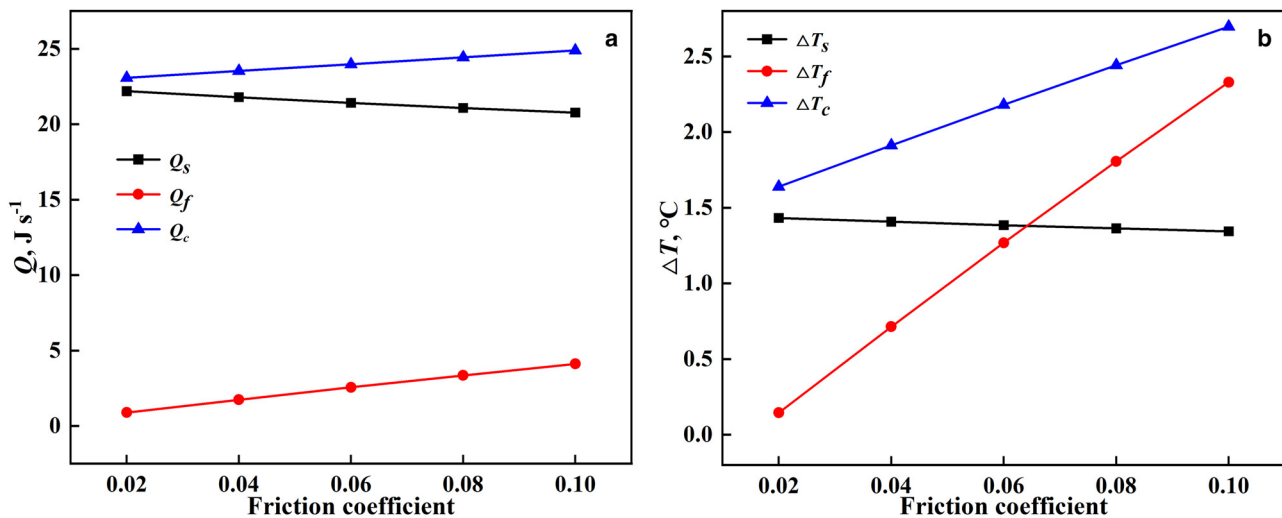


Figure 16. Model cutting heat and temperature rise vs friction coefficient between ice and the cutter: (a) cutting heat and (b) temperature rise of the cutter.

4.3.3 Thermal conductivity of the cutter

The effect of the thermal conductivity variation of the cutter on the cutting process and heat transfer efficiency is investigated in this study. Figure 15 illustrates that while the values of Q_s , Q_f and Q_c remain unchanged, an increase in the thermal conductivity of the cutter results in a decrease in the values of ΔT_f and ΔT_c . This decrease in temperature rise is due to the improved heat transfer efficiency. Therefore, it is recommended to use cutters with higher thermal conductivity in order to improve the heat transfer efficiency and lower the temperature rise during the cutting process.

4.3.4 Friction coefficient between ice and the cutter

Figure 16 demonstrates that the friction coefficient between the ice and the cutter during drilling is positively correlated with the values of ΔT_c and Q_c . When the friction coefficient increases from 0.02 to 0.1, ΔT_c and Q_c increase from 23.1 to 24.9 J s^{-1} and from 1.6 to 2.7 $^{\circ}\text{C}$, respectively. This is because an increase in the friction coefficient leads to a higher Q_f value, which, in turn, increases Q_c , T_c and T_f . The properties of ice and the cutting process are not affected by changes in the friction coefficient; thus, the values of Q_s and ΔT_s remain almost constant. As a result, it is recommended to minimize the friction coefficient between the ice and the cutter to reduce the cutting temperature.

5 Conclusions

A theoretical model was developed to investigate the cutting heat and the temperature of the cutter in the presence of drilling fluid during ice-core drilling. A series of tests were conducted to validate the theoretical model, and the maximum error between the experimental and the calculated results was <16%.

The drilling fluid can effectively reduce the temperature rise of the cutter, while its type and flow rate have little effect on the cutter temperature.

Increasing the rake angle and thermal conductivity of the cutter is recommended when drilling in warm ice since they have a negative correlation with the cutting heat and temperature.

The rotation speed of the drill bit, cutting depth, cutter width and the friction coefficient between the ice and the cutter are positively correlated with the cutting heat and temperature. Therefore, it is recommended to minimize their values.

Data. The data used for this study will be made available upon request. Please send all requests to yinqilei@jlu.edu.cn.

Acknowledgement. The authors acknowledge the financial support from the National Natural Science Foundation of China (project no. 41976213).

References

- Appl FC, Wilson CC and Lakshman I (1993) Measurement of forces, temperatures and wear of PDC cutters in rock cutting. *Wear* **169**(1), 9–24. doi:10.1016/0043-1648(93)90386-Z
- Azuma N, Tanabe I and Motoyama H (2007) Heat generated by cutting ice in deep ice-core drilling. *Annals of Glaciology* **47**, 61–67. doi:10.3189/172756407786857848
- Beer J and 6 others (1988) Information on past solar activity and geomagnetism from 10Be in the Camp Century ice core. *Nature* **331**, 675–679. doi:10.1038/331675a0
- Cao PL, Chen BY, Liu CP, Yang C and Talalay PG (2015) Experimental investigation of cutting temperature in ice drilling. *Cold Regions Science and Technology* **116**, 78–85. doi:10.1016/j.coldregions.2015.04.008
- Cao PL, Liu MM, Chen Z, Chen BY and Zhao Q (2018) Theory calculation and testing of air injection parameters in ice core drilling with air reverse circulation. *Polar Science* **17**, 23–32. doi:10.1016/j.polar.2018.06.005
- Cao PL, Chen Z, Cao HY, Chen BY and Zheng ZC (2020) Anti-icing performance of hydrophobic material used for electromechanical drill applied in ice core drilling. *Journal of Glaciology* **66**(258), 618–626. doi:10.1017/jog.2020.33
- Che D, Han P, Guo P and Ehmann K (2012) Issues in polycrystalline diamond compact cutter-rock interaction from a metal machining point of view – part I: temperature, stresses, and forces. *Journal of Manufacturing Science and Engineering, Transactions of the ASME* **134**(6), 064001. doi:10.1115/1.4007623
- Debnath S, Reddy MM and Yi QS (2014) Environmental friendly cutting fluids and cooling techniques in machining: a review. *Journal of Cleaner Production* **83**, 33–47. doi:10.1016/j.jclepro.2014.07.071
- Fang ZL and Obikawa T (2020) Influence of cutting fluid flow on tool wear in high-pressure coolant turning using a novel internally cooled insert. *Journal of Manufacturing Processes* **56**, 1114–1125. doi:10.1016/j.jmapro.2020.05.028
- Gorman JM, Abraham JP and Sparrow EM (2014) A novel, comprehensive numerical simulation for predicting temperatures within boreholes and the adjoining rock bed. *Geothermics* **50**, 213–219. doi:10.1016/j.geothermics.2013.10.001
- Javidikia M, Sadeghifar M, Songmene V and Jahazi M (2021) Low and high speed orthogonal cutting of AA6061-T6 under dry and flood-coolant modes: tool wear and residual stress measurements and predictions. *Materials* **14**(15), 4293. doi:10.3390/ma14154293
- John HL IV and John HL V (2006) *A Heat Transfer Textbook*, 3rd Edn. Cambridge, Massachusetts: Phlogiston Press.
- Kishawy HA, Dumitrescu M, Ng EG and Elbestawi MA (2005) Effect of coolant strategy on tool performance, chip morphology and surface quality during high-speed machining of A356 aluminum alloy. *International*

- Journal of Machine Tools and Manufacture* **45**(2), 219–227. doi:10.1016/j.ijmachtools.2004.07.003
- Komanduri R and Hou ZB** (2000) Thermal modeling of the metal cutting process. Part I: temperature rise distribution due to shear plane heat source. *International Journal of Mechanical Sciences* **42**, 1715–1752. doi:10.1016/S0020-7403(99)00070-3
- Komanduri R and Hou ZB** (2001a) Thermal modeling of the metal cutting process. Part II: temperature rise distribution due to frictional heat source at the tool–chip interface. *International Journal of Mechanical Sciences* **43**, 57–88. doi:10.1016/S0020-7403(99)00104-6
- Komanduri R and Hou ZB** (2001b) Thermal modeling of the metal cutting process. Part III: temperature rise distribution due to the combined effects of shear plane heat source and the tool–chip interface frictional heat source. *International Journal of Mechanical Sciences* **43**, 89–107. doi:10.1016/S0020-7403(99)00105-8
- Komanduri R and Hou ZB** (2001c) Analysis of heat partition and temperature distribution in sliding systems. *Wear* **251**(1), 925–938. doi:10.1016/S0043-1648(01)00707-4
- Kotlyakov VM, Lipenkov VY and Vasil'ev N** (2013) Deep drilling in central Antarctica and penetration into subglacial Lake Vostok. *Herald of the Russian Academy of Sciences* **83**(4), 311–323. doi:10.1134/S1019331613040035
- Li KM** (2006) *Predictive modeling of near dry machining: mechanical performance and environmental impact* (Dissertation). Georgia Institute of Technology.
- Lu ZH, Zhang DY, Zhang XY and Peng ZL** (2020) Effects of high-pressure coolant on cutting performance of high-speed ultrasonic vibration cutting titanium alloy. *Journal of Materials Processing Technology* **279**, 116584. doi:10.1016/j.jmatprotec.2019.116584
- Matoba S, Shimbori K and Shiraiwa T** (2014) Alpine ice-core drilling in the North Pacific region. *Annals of Glaciology* **55**(68), 83–87. doi:10.3189/2014aog68a020
- Mia M and Dhar NR** (2018) Effects of duplex jets high-pressure coolant on machining temperature and machinability of Ti–6Al–4V superalloy. *Journal of Materials Processing Technology* **252**, 688–696. doi:10.1016/j.jmatprotec.2017.10.040
- Motoyama H and 11 others** (2021) Deep ice core drilling to a depth of 3035.22 m at Dome Fuji, Antarctica in 2001–07. *Annals of Glaciology* **62**(85), 212–222. doi:10.1017/aog.2020.84
- Ortega A and Glowka DA** (1984) Frictional heating and convective cooling of polycrystalline diamond drag tools during rock cutting. *Society of Petroleum Engineers Journal* **24**(2), 121–128. doi:10.2118/11061-PA
- Pattyn F** (2010) Antarctic subglacial conditions inferred from a hybrid ice sheet/ice stream model. *Earth & Planetary Science Letters* **295**, 451–461. doi:10.1016/j.epsl.2010.04.025
- Shan CW, Zhang X, Shen B and Zhang DH** (2019) An improved analytical model of cutting temperature in orthogonal cutting of Ti6Al4V. *Chinese Journal of Aeronautics* **32**(3), 759–769. doi:10.1016/j.cja.2018.12.001
- Shokrani A, Dhokia V and Newman ST** (2012) Environmentally conscious machining of difficult-to-machine materials with regard to cutting fluids. *International Journal of Machine Tools and Manufacture* **57**, 83–101. doi:10.1016/j.ijmachtools.2012.02.002
- Steinhilber F and 13 others** (2012) 9,400 years of cosmic radiation and solar activity from ice cores and tree rings. *Proceedings of the National Academy of Sciences of the United States of America* **109**, 5967–5971. doi:10.1073/pnas.1118965109
- Takeuchi N and 6 others** (2004) A report on ice core drilling on the western plateau of Mt. Belukha in the Russian Altai Mountains in 2003. *Polar Meteorology and Glaciology* **18**, 121–133.
- Talalay PG** (2014) Drill heads of the deep ice electromechanical drills. *Cold Regions Science and Technology* **97**, 41–56. doi:10.1016/j.coldregions.2013.09.009
- Talalay PG** (2016) *Mechanical Ice Drilling Technology*. Singapore: Springer Geophysics.
- Talalay PG and 7 others** (2015) Ice-core drilling problems and solutions. *Cold Regions Science and Technology* **120**, 1–20. doi:10.1016/j.coldregions.2015.08.014
- Truffer M and 5 others** (1999) Subglacial drilling at Black Rapids Glacier, Alaska, USA: drilling method and sample descriptions. *Journal of Glaciology* **45**(151), 495–505. doi:10.3189/S0022143000001350
- Veiga F, Arizmendi M, Jiménez A and Val AGD** (2021) Analytical thermal model of orthogonal cutting process for predicting the temperature of the cutting tool with temperature-dependent thermal conductivity. *International Journal of Mechanical Sciences* **204**, 106524. doi:10.1016/j.ijmecsci.2021.106524
- Wang YQ and 5 others** (2020) Modeling of temperature distribution in turning of Ti–6Al–4V with liquid nitrogen cooling. *The International Journal of Advanced Manufacturing Technology* **107**, 451–462. doi:10.1007/s00170-020-05093-4
- Xu GQ and 7 others** (2020) Tunable analog thermal material. *Nature Communications* **11**(1), 6028. doi:10.1038/s41467-020-19909-0
- Yao DT, Liu QY, Kang CS, Jiao ZN and Zeng HY** (2008) Bacteria variabilities in a Tibetan ice core and their relations with climate change. *Global Biogeochemical Cycles* **22**, GB4017. doi:10.1029/2007GB003140
- Zhang ZZ and 5 others** (2020) Simulation and experimental study on temperature and stress field of full-sized PDC bits in rock breaking process. *Journal of Petroleum Science and Engineering* **186**, 106679. doi:10.1016/j.petrol.2019.106679
- Zhong ZP and 10 others** (2021) Glacier ice archives nearly 15,000-year-old microbes and phages. *Microbiome* **9**(1), 160. doi: 10.1186/s40168-021-01106-w